Article

Systematic Characterization of Gas Phase Binary Pre-Nucleation Complexes Containing HSO + X, [X = NH, (CH)NH, (CH)NH, (CH)N, HO, (CH)OH, (CH)O, HF, CHF, PH, (CH)PH,(CH3)2PH, (CH3)3P, H2S, (CH3)SH, (CH3)2S, HCl,(CH3)Cl)] - A Computational Study

Paolo Sebastianelli, Rodolfo G. Pereyra, and Pablo M. Cometto

Just Accepted

1
2
3
4
5
6
7
8
9
10
11
12
13
14
15
16
17
18
19
20
21
22
23
24
25
26
27
28
29
30
31
32
33
34
35
36
37
38
39
40
41
42
43
44
45
46
47
48
49
50
51
52
53
54
55
56
57
58
59
60

Systematic Characterization of Gas Phase Binary Pre-Nucleation Complexes Containing H_2SO_4 + X, [X = NH_3, $(CH_3)NH_2$, $(CH_3)_2NH$, $(CH_3)_3N$, H_2O, $(CH_3)OH$, $(CH_3)_2O$, HF, CH_3F, PH_3, $(CH_3)PH_2$, $(CH_3)_2PH$, $(CH_3)_3P$, H_2S, $(CH_3)SH$, $(CH_3)_2S$, HCl, $(CH_3)Cl$)] - A Computational Study

Paolo Sebastianelli[1,2] , Pablo M. Cometto[2,3], Rodolfo G. Pereyra*[1,4]

[1] Fa.M.A.F., Universidad Nacional de Córdoba, Medina Allende s/n, Ciudad Universitaria, X5000HUA Córdoba, Argentina.

[2] FCEyN, Universidad Nacional de La Pampa. Uruguay 151 - (6300) Santa Rosa - La Pampa, Argentina.

[3] INCITAP-CONICET. Atmospheric Chemical Physics Laboratory. Uruguay 151 - (6300) Santa Rosa - La Pampa, Argentina.

[4] IFEG-CONICET, Medina Allende s/n, Ciudad Universitaria, X5000HUA Córdoba, Argentina.

Corresponding Authors

E-mail: pereyra@famaf.unc.edu.ar Tel: +54 9 351 4334051 int. 254

E-mail: spaolo@famaf.unc.edu.ar

1
2
3
4
5
6
7
8
9
10
11
12
13
14
15
16
17
18
19
20
21
22
23
24
25
26
27
28
29
30
31
32
33
34
35
36
37
38
39
40
41
42
43
44
45
46
47
48
49
50
51
52
53
54
55
56
57
58
59
60

Abstract

A systematic characterization of gas phase binary pre-nucleation complexes between H_2SO_4 (SA) and other molecules present in the atmosphere (NH_3, $(CH_3)NH_2$, $(CH_3)_2NH$, $(CH_3)_3N$, H_2O, $(CH_3)OH$, $(CH_3)_2O$, HF, $CH_3 F$, PH_3, $(CH_3)PH_2$, $(CH_3)_2PH$, $(CH_3)_3P$, H_2S, $(CH_3)SH$, $(CH_3)_2S$, HCl, $(CH_3)Cl$) has been carried out using the ωB97X-D/6-311++(2d,2p) method at the DFT level of theory. A relationship between the energy gap of the SA's LUMO and the partner molecule's HOMO, and the increasing number of methyl groups -CH_3 in the SA's partner molecule is provided. The binding energies of the bimolecular complexes are found to be related to the electron density in the Hydrogen Bond Critical Point, the HOMO-LUMO energy gap, the nature of the hydrogen acceptor atom and the frequencies shift of acid OH bonds. The results show how the frontier orbitals compatibility determines the binding energy and that the properties of SA's OH bond which remains free of interactions are affected by the bimolecular adduct formation.

1. Introduction

One of the mechanisms of secondary atmospheric aerosols formation starts with the gas-to-particle process that leads to pre-nucleation molecular clusters generation. New atmospheric particles formation is a phenomenon which has been detected in numerous locations around the world[1-5], including areas with a pristine atmosphere, e.g., coastal areas[6], Antarctic/Arctic[7] zones, remote forest[8], semi-rural locations with very low pollution levels and heavily polluted cities[9-10]. Nucleation of gas phase precursors and subsequent condensational growth are crucial steps of this process.

Adjustments to the descriptive nucleation models are required to reach reasonable agreement with field observations. The simulation of nucleation over a very wide range of atmospheric conditions is an important tool to obtain reliable results. Recent work of Dunne et al.[11] offers a new understanding of global particle formation as based almost entirely on ternary rather than binary nucleation, with ions playing an important but subdominant role. The results of these authors suggest that about 43% of cloud-forming aerosol particles in the present-day atmosphere is originated by nucleation. Detailed mechanisms of pre-nucleation clusters formation are needed to develop nucleation models[5]. Unfortunately these mechanisms have not yet been completely understood.

Since the 90s experimental evidence has shown that gas phase acids as, for example, the sulfuric acid or methane sulfonic acid, are protagonists of the pre-nucleation of new atmospheric particles from gas phase conversion. The earlier stages of molecular clusters formation has been studied in several projects with the use of different equipments: chemical ionization mass spectrometers[12], condensation particle counters[13] or a group of instruments present in the recent CLOUD project[14]. The evidence indicates that atmospheric particle formation from gas phase not only involves acidic molecules and water, but also amines, low-volatile organic compounds (LVOCs), ions and oxidized organic molecules. Theoretical predictions obtainables by DFT and other quantum-mechanics calculations have been developed initially[15-16] to describe the formation of H_2SO_4 hydrates

and the corresponding thermodynamic functions. Later, the exploration has been expanded to include the stabilization effects caused by the other kind of molecules mentioned above. Kurten et al.[17] predicted that ammonia and alkylamines stabilize the clusters containing H_2SO_4 (and H_2O) by ammonium salts formation. Berndt et al.[18] have experimentally estimated the enhancement of the nucleation rates in the presence of tert-butylamine, and confirmed the theoretical finding by Loukonen et al.[19] that amines are more efficient than ammonia in stabilizing sulfuric acid-containing clusters. Furthermore, Berndt and coworkers[20] found that dimethyl amine enhanced nucleation rates with sulfuric acid more efficiently than products of monoterpene oxidation.

Methanesulfonic acid is another example of acidic molecule which takes place in particle formation processes[21-27]. It is formed from the oxidation of organosulfur compounds that originate from biological processes, biomass burning, industrial operations, and agricultural activities[28-29]. A number of studies have been performed to define the role of the methanesulfonic acid in particle formation in the gas phase. This phenomenon has been extensively studied, from experimental and theoretical point of views. Dawson and coauthors[26], for example, reported a combination of experimental and theoretical analysis of new particle formation from mixtures of methanesulfonic acid, amines, and water. Bork and coworkers[30] investigated the effect and role of methanesulfonic acid in the formation of molecular clusters in atmospheres containing various quantities of methanesulfonic acid, sulfuric acid and dimethyl amine. Chen and coworkers[24] conducted comprehensive experiments and used a quantum chemical approach, to investigate the effect of water on new particle formation (NPF) and the growth from MSA with ammonia and a series of amines including methylamine and dimethylamine. In a recent work, Kumar and Francisco[31] performed Born-Oppenheimer molecular dynamics simulations and density functional calculations to investigate the ion pair particle formation from methanesulfonic acid and NH_3, CH_3NH_2 and $(CH_3)_2NH$ at the air-water interface.

In spite of much work has been done to characterize the interactions between H_2SO_4 (SA) or $(CH_3)SO_3H$ (HMSA) and the aforementioned compounds, a systematic analysis approach to the

problem may help to reach new insights concerning the contribution from the acidic precursors in particle formation processes. In the present work, we have considered, SA a *pivot* molecule able to donate hydrogen atoms to H-acceptor molecules, as well as to form multi-point non-covalent interactions through the S=O and S-OH functionalities. The latter aspect is well-known and it is important for the cases in which single or double hydrogen atom transfer (HAT) between SA and a partner molecule could occur[32-33]. The effects of the nature acid proton acceptor atom on the binding energy (hereafter E_b), have been studied carrying out the calculations over a series of gas-phase binary molecular complexes characterized by SA partners with hydrogen acceptor atoms from the second (N, O, F) and third (P, S, Cl) chemical Period. To the best of our knowledge, excluding the clusters formed by SA - amines[18-20], SA - methanol[52] and SA - dimethylether[53], the bimolecular adducts constituted by SA and the others partner molecules that we propose in this study have not been studied yet through a step by step procedure of a systematic approach.

The E_b of complexation have been analyzed and the hydrogen bond (hereafter *HB*), formed between SA's acid proton and the hydrogen acceptor atom (hereafter A), has been characterized. To complement previous studies in the literature, the results are discussed in terms of the Gibbs Free Energy of adducts formation, E_b, Frontier Molecular Orbital characterization, electron density to the Hydrogen Bond Critical Point, frequencies shift of sulfuric acid OH bonds.

2. Theoretical Methods

2.1 Computational Details

The bimolecular systems geometry optimizations, vibrational analysis and thermochemical parameters calculations were performed using the GAMESS software package[34-35]. Calculations at the DFT level of theory, employing ωB97X-D long-range corrected (LC) hybrid functional[36], were carried out with 6-311++(2d,2p) basis set. Single point calculations at the CCSD(T)/aug-cc-pVTZ on the DFT

optimized geometries have been performed in all cases except for N3 and P3, due to memory issues. N3 and P3 binding energies have been calculated at the CCSD(T)/aug-cc-pVDZ level of theory. The ωB97X-D functional includes empirical atom–atom dispersion correction. The choice of the computational method is based on the satisfactory performance of the ωB97X-D functional on the calculation of binding energies of atmospheric electroneutral clusters, described in two benchmark papers of the authors Elm and coworkers[37-38]. Due to the qualitative nature of our work, and computational issues, it has been opted, as first step of analysis, for reaching an equilibrium between computational effort and accuracy of the results, choosing 6-311++(2d,2p) basis set. This choice has been motivated taking into account another Elm and coworkers article[39] within which they show how reducing the basis set used in the geometry and frequency calculation from 6-311++G(3df,3pd) → 6-31++G(d,p) implies a significant speed-up in computational time and only leads to small errors in the thermal contribution to the Gibbs free energy. Our work has been designed speculating that the systematic approach would have allowed conclusions to be drawn independently from the calculation inherent errors, since the same study scheme has been applied in all cases. No BSSE (Basis Set Superposition Error), CP (CounterPoise) method, or scaling factor for the vibrational frequencies calculations, have been applied due to the extension of the basis set and the comparative and qualitative nature of this study. Vibrational frequency analysis was performed, in harmonic approximation, to confirm all stationary points as local minima structure. The geometrical parameters analysis and the characterization of frontier molecular orbitals have been performed using MacMolPlt software[40]. Once the molecular system wavefunctions have been determined by GAMESS, the AIM analysis has been performed using the MultiWfn software[41].

Since the goal of this study is not exploring the Potential Energy Surface (PES) as much as possible and the molecular systems that have been studied are rather simples (low number of possible conformations), the geometries associated to a minimum of energy have been searched mixing chemical intuitions with the data, already confirmed by other authors, available in other bibliography

works. With the purpose of drawing some systematic conclusion, the systematic approach has been

adopted to search the other structures. For example, for the N complexes group the data available in the

literature are exhaustive[42-44]. The equilibrium geometries have been reproduced to check the method,

energetics comparable with those of the literature have been obtained. Starting from these equilibrium

geometries we have intentionally mimicked those belonging to N group to generate the calculation start

points of the P complexes group. The other cases have been handled in the same way as far as possible.

2.2 Systematic Study Design

This study encloses molecular systems already studied and new ones deliberately elected to

gain new physico-chemical intuitions on the SA bimolecular complexation. Although a number of

different SA bimolecular systems, characterized by different hydrogen acceptor atoms A, have already

been studied, to the best of our knowledge, it does not exist an article within which a systematic

approach is proposed to characterize the influence of the A nature on the H-bond and the binding

process. The relationships between characterization parameters and the associated trends, that have

already been investigated in other studies, have been taken into account to check the proposed method.

Nevertheless, more than the relationships between the chemico-physical parameters, the first goal of

this work is the description of the systematic trends by the application of a systematic method. Building

the big picture, step by step, should permit to detect probable counterintuitive results. Table 1 shows

the study design considered. Binary molecular complexes containing only one SA molecule have been

studied (see Figure 1a as an example). With the objective of studying the effects of hydrogen acceptor

atoms' chemical nature on the E_b, three SA partners molecules characterized by hydrogen acceptor

atoms from the second (N,O,F) and three from the third (P,S,Cl) chemical period have been chosen.

They are Ammonia (NH_3), Water (H_2O), Fluorhydric Acid (HF), Phosphine (PH_3), Sulfhydric Acid

(H_2S) and Chlorhydric acid (HCl) respectively. To change the degree of substitution, the hydrogen

atoms belonging to the SA partner molecules have been substituted by an increasing number of methyl

groups -CH_3 and a range of 12 other binary clusters has been studied. The derived SA partners are:

$(CH_3)NH_2$, $(CH_3)_2NH$, $(CH_3)_3N$, $(CH_3)OH$, $(CH_3)_2O$, $(CH_3)F$, $(CH_3)PH_2$, $(CH_3)_2PH$, $(CH_3)_3P$,

$(CH_3)SH$, $(CH_3)_2S$, $(CH_3)Cl$. The aim of this substitution was to take into account the positive

inductive effect (+I: transmission of charge on a chain of atoms via electrostatic induction), due to the

substituent -CH_3, groups on the bonds responsible for the cluster's formation. The identification label

for binary complexes is AX type: A is the chemical symbol of the hydrogen acceptor atom in SA's

partner molecule and X is the number of -CH_3 methyl substituent groups in SA partner molecule (e.g.

N2 is the identification label for the binary cluster formed by one SA molecule and $(CH_3)_2NH$).

The following geometrical parameters have been taken into account in order to describe the

nature of the binding process between SA and the AX partner molecules: the length of the hydrogen

bond and the other non-covalent interaction d_{HB} and d_{NCI_I}, the d_{OH_I} and d_{OH_II} bond distances (see

Figure 1a). The variations of d_{OH_I} and d_{OH_II} were labeled as Δd_{OH_I} and Δd_{OH_II}, respectively.

In order to identify the thermodynamic spontaneity of the complexation process, the free Gibbs

energy change between the separated molecules and the bimolecular system have been calculated at T

= 298.15 K and P = 1 atm.

The Binding Energy E_b has been calculated as the difference in electron energy of the

fundamental states:

$$E_b = |E_{BC} - (E_{SA} + E_{AX})| = |\Delta E_0|$$

where E_{BC} is the energy of the binary complex, E_{SA} is the energy of sulfuric acid and E_{AX} is the

energy of the hydrogen acceptor molecule (A = acceptor atom = N, O, F, P, S, Cl).

Among the different aspects that may regulate the interaction between molecular systems the

energy gap between their frontier molecular orbitals and the topological properties of the electron

density of the separated molecules and those resulting from the adducts formation play a fundamental

role. For this reason the AIM[45] (Atoms In Molecules) and the FMO (Frontier Molecular Orbitals)

analysis have been coupled to study the relationship between the electron density in the hydrogen bond critical point, E_b and the molecule partner HOMO and SA's LUMO energy gaps before their binding. The positive inductive effect +I of the -CH_3 substituents present in the SA partner molecules has also been studied, hypothesizing that the number of -CH_3 can affect the electron density in hydrogen bond zones. In the present work BCP_{HB} is the critical point associated to the *HB*. The value of the electron density in BCP_{HB} has been labeled ρ_{BCP_HB}. BCP_I and BCP_{II} identify secondary Non Covalent Interactions: NCI_I and (when it is possible) NCI_{II} respectively. Figure 1a shows, as an example, the location of BCP_I and BCP_{II} in a complex. Ring Critical Points (RCP) have been also calculated and they are shown (if they exist) in Figure 1b. Finally, $\rho(\mathbf{r}_c)$ calculations for the critical points associated with OH_I and OH_{II} bonds NCI_I, NCI_{II}, RCP_I, RCP_{II}, named ρ_{OH_I}, ρ_{OH_II}, ρ_{NCI_I}, ρ_{NCI_II}, ρ_{RCP_I} and ρ_{RCP_II} respectively, were carried out.

Dimitrova and Galabov[46-47] have pointed out the existence of a linear correlation between the Electrostatic Potential[48] V_H calculated in the position of the hydrogen nucleus which is involved in a H-bond and the binding energy E_b associated to the bimolecular gas phase clusterization between ammonia and other partner molecules. Inspired by their works the Electrostatic Potential V_H at the SA nucleus *H* involved in a H-bond has been also calculated using the Multiwfn software.

Regarding the OH_I of the sulfuric acid, it is expected[49] that the hydrogen bond formation leads to a stretching of the of acid SO-H bond. For this reason the stretching frequencies $\Delta\nu_{OH\_I}$ and $\Delta\nu_{OH\_II}$ have been calculated.

3. Results and Discussion

The optimized molecular structures are shown in Figure 1b) along with the AIM analysis molecular graph representation. Table 2 is provided from the beginning of this section to summarize and order the simulations data according to the different kind of analysis performed on the molecular

systems.

3.1 Non-Covalent Interactions

We have focused on the H-bonds formed between A (N, O, F, P, S, Cl) and the SA proton in OH_I bond. This H-bond is characterized by an interaction length labeled d_{HB} and a Bond Critical Point identifiable as BCP_{HB}. Although the interaction between SA proton and N in the N1, N2 and N3 cases may lead to salt formation[17], the same notation has been adopted (i.e. d_{HB}), then, once analyzed the proposed bond descriptors, the actual nature of these interactions will be discussed. Excepting N0 and P0, all complexes present at least an additional bond critical point which is associable to an extra NCI bond that appears as a consequence of the molecular association. We name these additional interactions as NCI_n *(n = I, II, III ...)* and the corresponding bond critical point as BCP_n. When more than one NCI bond is formed Ring Critical Points RCP could appear. The position of the RCP reveals the stability of an interaction: its proximity to a bond path means that this bond path is unstable, such as it can be observed for N0 and P1 in the Figure 1b. In the Figure 1b can also be observed that, Cl1, O2, S2, N3 and P3 complexes, present a BCP_I associated to a NCI_I and two RCP.

3.2 Geometrical parameters

The hydrogen bond lengths, d_{HB}, for the second and third Chemical Period hydrogen acceptor atoms are shown in Table 2 (column 1). Due to the change of Chemical Period the values of d_{HB} can be divided in two intervals (in Å): 1.05 (N2) < d_{HB}< 1.84 (F0) and 2.10 (S2) < d_{HB}< 2.33 (Cl0) respectively. In each case the increasing of the degree of substitution of the hydrogen acceptor molecule leads to a shortening of d_{HB}. Concerning to N acceptor atom group, the complexation process leads to the extraction of OH_I proton with a consequent methyl, dimethyl and trimethyl ammonium formation (N1, N2, N3 complexes). A new N-H covalent bond is obtained with consequent *HB* disappearance.

The data associated to the OH_I bond show that the complexes formation makes this bond

longer. It occurs in all the studied cases. The OH_I bond variation Δd_{OH_I} values span between a minimum of 0.0132 (Cl0) and a maximum of 0.0644 (N0) Å. For these cases the OH_I proton transfer does not occur. On the contrary for N1 (0.6434), N2 (0.7194) and N3 (0.5334) cases Δd_{OH_I} assumes bigger values suggesting a OH_I bond rupture. The same conclusion can be argued if the d_{HB} values of these three cases is analyzed (d_{HB_N1} = 1.06, d_{HB_N2} = 1.05, d_{HB_N3} = 1.08 Å) because they approach the value of 1 Å whereas this parameter for the rest of the cases takes values between 1.58 (O2) and 2.33 (Cl0). These geometrical parameters are not specific descriptors to define a proton transfer process, nevertheless in the context of a systematic study, they can support that for N1, N2 and N3 a salt formation occurs.

Concerning the OH_{II} bond a shortening ($\Delta d_{OH\_II} < 0$) is observed for all the binary complexes formation except for the F0 and Cl0 (Δd_{OH_II}(F0) = 0.0004 Å; Δd_{OH_II}(Cl0) = 0.0003 Å). This suggests that, during the complexation process, the alkyl halides act in a different way respect the other SA partner molecules. Since the calculated Δd_{OH_II} quantities are really low in value for F0 and Cl0 cases it is necessary to validate the conjecture by an analysis of OH_{II} physico-chemical parameters (e.g. the electron density in OH_{II} bond critical point or the stretching frequency ν_{OH_II}).

3.3 Thermochemical quantities and binding energy

An analysis of the thermodynamic function trends (i.e ΔG, ΔH, $T\Delta S$) was performed for the considered complexes and the results are depicted in the Figure 2. It has to be reminded that $\Delta G < 0$, as result, do not necessarily imply that the complexes are formed in the atmosphere. The concentration of the interacting monomers is also relevant, but it is not a study object in this work.

As can be observed, the formation of H_2S-H_2SO_4 (S0), PH_3-H_2SO_4 (P0), HCl-H_2SO_4 (Cl0) and CH_3Cl-H_2SO_4 (Cl1) systems, according to the calculations, seems to be not spontaneous process at 298.15 K and constant pressure of 1 atm. It can be observed that the $T\Delta S$ contribution is similar in almost all the cases. Figure 2 shows that the ΔG displays the same trend as the ΔH. A linear

relationship between ΔG and $\Delta H = \Delta E + \Delta nRT$, that is shown in the plot embedded in the same figure, has been found. If the enthalpic change, ΔH, is not enough to overcome the entropy decreasing due to the bimolecular association process (loss of translational and rotational degrees of freedom) the process is not spontaneous. Hence, the free energy stabilization is associated with the decreasing of ΔH. Considering that the formation of bimolecular complexes is characterized in each case by a constant ΔnRT ($\Delta n = 1$; T = 298.15 K) = -0.5925 kcal/mol, the enthalpic contribution is mainly due to the total internal energy change ΔE. The value of ΔG_{O0} = -3.31 kcal/mol for O0 case is comparable with the experimental data of -3.6 kcal/mol (also shown in Figure 2) provided by Eisele and Hanson[51]. Elm et al.[42] have optimized the geometries of N0, N1, N2 and N3 with the 6-31++G(d,p) basis set at M06-2X, PW91 and ωB97X-D level of DFT theory. They have obtained the binding energies after a CCSD(T)-F12a/VDZ-F12 calculation. They have provided the values of ΔG in kcal/mol at 298.15 K and 1 atm: ΔG_{N0} = -5.2, ΔG_{N1} = -8.2, ΔG_{N2} = -11.9, ΔG_{N3} = -12.2 (see Figure 2).

In this work, although no BSSE (Basis set superposition error), CP (CounterPoise) method, or scaling factor for the vibrational frequencies calculations have been applied, the ΔG values obtained for N0, N1, N2 and N3, O1 and O2 display a trend comparable to the Elm et al. works[52-53].

To the best of our knowledge, no previous thermodynamic calculations were performed for the rest of the chosen complexes.

In Figure 3a the E_b for each bimolecular system, grouped according to the Table 1 criteria, have been plotted. The E_b values related to the Nitrogen group are higher than the others. The cause of this result is the extra stabilization due to the transfer proton process and the consequent methyl, dimethyl and trimethyl-ammonium salts formation. This aspect will be taken into account, again, in the following paragraph. The substitution of H atoms by an increasing number of -CH$_3$ groups leads to bigger values of E_b in each subgroup, with the exception of the F group. Nevertheless this exception has not been registered for the other halogenated SA's partner considered in Cl0 and Cl1 complexes.

This aspect will be clarified during the discussion of the AIM data analysis.

The comparison between adducts with hydrogen acceptor atoms belonging to different chemical Periods does not produce fully systematic results. However, some general observations could be pointed out. Comparing binary complexes characterized by hydrogen acceptor atoms belonging to the same Chemical Group in the periodic table, it is possible to observe that: the complexes belonging to the N group show bigger binding energies than the complexes belonging to the P group. The same result has been obtained for the complexes characterized by hydrogen acceptor atoms belonging to the VIA and VIIA chemical group: the O complexes set shows bigger binding energies than that S set and the F set bigger than Cl set, respectively. In summary, for hydrogen acceptor atoms belonging to the same group of the periodic table, E_b decreases as the period increases.

3.4 Molecular Orbitals and AIM analysis

The results obtained by Frontier Molecular Orbitals and AIM analysis are provided in a joined discussion to unravel the three-point relationship between the binding energies, the HOMO-LUMO energy gap and the electron density topology. Shared interactions (covalent bonds) are associated with relatively large values of ρ_{BCP_HB} and negative values of the Laplacian ($\nabla^2\rho_{BCP\_HB} < 0$). Conversely, non-covalent interactions are characterized by small values of ρ_{BCP_HB} and a positive curvature of the density along the bond path ($\nabla^2\rho_{BCP\_HB} > 0$)[45].

Figure 3b shows a clear linear relation between E_b versus ρ_{BCP_HB}. This is a result that different authors[55-58] have already highlighted. The strength of the hydrogen bonds could be determined according to the Popelier[59] criterion, which states that the electron density and its Laplacian, for a hydrogen bond, range from 0.002 to 0.040 a.u. and from 0.024 to 0.139 a.u. respectively. The major part of the bimolecular complexes shows electronic density in the considered ranges and positive

values of the Laplacian. N0, O0, O1, O2 and P3 cases are characterized by electronic density and Laplacian bigger than the upper values corresponding to the criterion, showing strong hydrogen bonds. For the N1, N2 and N3 cases the Laplacian $\nabla^2\rho_{BCP\_HB}$ is negative corresponding to a covalent bond formation[45]. In these cases the proton transfer on the acceptor atom N leads to the formation of a new N-H covalent bond and the salt formation.

In a cause-effect interpretation it can be argued that the increase of electron density in the hydrogen bond region makes the interaction stronger and this results in a bigger value of E_b. The substitution of H atoms by an increasing number of -CH$_3$ groups and the consequent increase of +I effect onto the hydrogen acceptor atom seems to lead to bigger values of ρ_{BCP_HB} in each subgroup, with the exception of the F group. The reason has been thought to reside in the frontiers molecular orbitals compatibility between SA and the partner molecules.

For this reason a FMO analysis has been performed on isolated SA molecule, isolated AX and on the formed binary molecular complexes. In Figure 3d the energy gap ΔE_{HL} between the partner molecule HOMO$_{AX}$ and the sulfuric acid LUMO$_{SA}$ can be seen for each bimolecular system. The increase of -CH$_3$ substituents number in a hydrogen acceptor molecule is associated to a reduction of ΔE_{HL}.

For a better visualization, details about the MOs are provided in the diagram of Figure 4. The sulfuric acid's frontier molecular orbitals has the following energies: E_{LUMO} (H$_2$SO$_4$) = 0.028 a.u. and E_{HOMO}(H$_2$SO$_4$) = -0.429 a.u. As it is shown in the Figure 4a), LUMO$_{SA}$ orbital is characterized by two big lobes on the two hydrogen atoms. These are the molecular sites, which are available for interacting with the electron pair of the hydrogen acceptor atom. HOMO$_{AX}$ is generally characterized by the biggest lobes on the hydrogen acceptor atom independently from the number substituent methyl groups (see two examples shown in Figure 4b). This is a general result except when the hydrogen acceptor

atom is F. The $(CH_3)F$ HOMO, shown in Figure 4c, is characterized by the biggest molecular orbital lobes on the methylic hydrogen atoms which is an unfavorable aspect for the hydrogen bond formation.

The reduction of ΔE_{HL} facilitates the formation of new bimolecular MOs crossing along the hydrogen bond region[54] resulting in an increase of ρ_{BCP_HB} as it is observable in Figure 3e where inverse proportional relation between these two parameters occurs for adducts with the same hydrogen acceptor atom. The plot shows two groups, one for each chemical period.

From the analysis of the results so far discussed it can be may deduced that an inverse proportional relation between E_b and ΔE_{HL} can be raised. Figure 3f confirms this conjecture, except if the cases S2-P3, O2-N0, F0-F1 are compared. It can be pointed out that there are two aspects that could be highlighted: the importance of the ΔE_{HL} (before and after the complexation process) and the overlap percentage between the MOs. As first step of analysis, in our work, the attention has been focussed to the ΔE_{HL} between the separated molecule. It is believed, after the initial electrostatic interaction between the two molecules, being the basis for the subsequent evolution of the pre-nucleation process. For example, if the F0-F1 cases are compared, the inverse proportional relation between E_b and ΔE_{HL} does not occur even if a F1's reduced ΔE_{HL} can be relationed to a bigger value of ρ_{BCP_HB}. As already described, the $(CH_3)F$ HOMO, characterized by the biggest molecular orbital lobes on the methylic hydrogen atoms, could be the reason of this situation. The $\rho_{BCP\_HB}(F1) > \rho_{BCP\_HB}(F0)$ but $\rho_{NCI\_I}(F1) < \rho_{NCI\_I}(F0)$ and this aspect could affect the overall amount of E_b.

Since the studied SA's complexation processes are hydrogen bond-mediated, could be useful take in account a H-bond puzzle proposed by Gilli and coworkers[49-50]. Trying to find the intercorrelation among the physical quantities that characterizes the H-bond they wondered[50]: 'Which physical quantity, out of the many intercorrelated ones, is the independent variable that drives the H-bond strength and, in turn, all its other associated properties?'. They summarized[49] ".. the results obtained, that constitute the empirical laws governing the H−bond, and

show that the driving variable sought has to be identified in the acid-base indicators (proton affinities in the gas phase and related acid-base dissociation constants in solution) of the H-bond donor and acceptor'.

Although the main objective of this work is not to solve the H-bond puzzle that Gilli et al.[49-50] have posed in their work it could be reasonable to think that ΔE_{HL} is one of the candidates to be the variable that drives the H-bond strength. The ΔE_{HL} is predetermined by the nature of the two molecules before the complexation process, and, once the complex is formed, the bimolecular HOMO-LUMO energy gap could drive the electronic density redistribution.

Taking into account only one critical point along the hydrogen bond path, the discussion of the trends of aforementioned parameters could be arguable because it implies considering partial information. To complement this aspect the electron density maps on the H-bond planes, defined by Acceptor-Hydrogen-Donor atoms, have been analyzed for the different cases. This analysis helps the interpretation of the electron density changes in the hydrogen bonds regions. Figure 5 shows descriptive examples. The effect of increasing substitution degree in SA partner molecule is shown in the upper part of Figure 5. P1, P2 and P3 cases are drawn. It can be observed as the -CH$_3$ substituents number increases the electron density value in hydrogen bond zone increases. This is a general result which occurs in each studied group. The lower part of Figure 5 displays, as an example, the comparison between N0 and O2, P3 and S2 that are the adducts characterized by the highest degree of substitution. The analysis of the colored regions shows the decreasing order N0 > O2 > P3 > S2 in H-bond region electron density coinciding with the values trend of ρ_{BCP_HB} for these cases: 0.0683 a.u. > 0.0599 a.u. > 0.0417 a.u. > 0.0390 a.u..

A discussion can be added for what concern O2 and S2, since studies on similar systems exist in the literature[60-61]. Tang and coworkers[60] have investigated the O–H⋯O and O–H⋯S hydrogen

bonds in the alcohol–ethylene oxide (EO) and alcohol–ethylene sulfide (ES) complexes in the gas

phase by FTIR spectroscopy. They have also performed DFT calculations to determine the stable

structures and interaction energies of the complexes, with ωB97X-D functional using aug-cc-pVTZ

basis set on all atoms except for the sulfur atom. Du et al.[61] chose MeOH, EtOH, and 2,2,2-

trifluoroethanol (TFE) as the hydrogen bond donors and DME, DMS as the hydrogen bond acceptors.

They have compared the strength between the O–H⋯O and O–H⋯S hydrogen bonds and the strength

of the complexes, as they changed the donor from weak (MeOH) to strong (TFE). They also have

implemented a DFT study carried out with ωB97X-D, using the aug-cc-pVTZ basis set on all atoms

except for the sulfur atom. The AIM analysis provides in our study is in accordance with those

provided by Tang and Du, as well as the trends of the binding energies: bigger values of ρ_{BCP_HB} and E_b

correspond to O-H⋯O cases. Some differences have been encountered analyzing the redshift $\Delta\nu_{OH}$

and they are discussed in the "Stretching Frequency Shift" paragraph.

3.5 Electrostatic Potential

The authors Dimitrova and Galabov[46-47] have studied different molecular systems to determine

the relation between Electrostatic Potential[48] V_H and the binding energy E_b. They have found a linear

correlation between both parameters.

In their study, they have analyzed a series of complexes involving different types of proton

donor molecules and ammonia as a model proton acceptor. In this study we chose the same proton

donor site in each case (i.e. SA) while different proton acceptor molecules AX have been used as

partner compounds.

Nevertheless the linear correlation between V_H and E_b has been confirmed. Further bigger

values of E_b are associated with more negative values of Electrostatic Potential V_H at the position of the

SA's acid proton nucleus. The result is shown in Figure 3c. The negative value of V_H means that the

electronic contributions to the total electrostatic potential is bigger than the nuclear one. The increase of the negative value of V_H means that the electron density in the H-bond region increase. It is a further indirect demonstration of the ρ_{BCP_HB} raise.

3.6 Stretching Frequency Shift

As the hydrogen bond becomes stronger the H-Donor bond weakens and stretches[49]. This aspect can be analyzed from two points of view: decreasing electron density ρ_{OH_I} or the *redshift* of the ν_{OH_I} stretching frequency. The O-H stretching frequency ν_{OH_I} of an isolated SA molecule has been calculated and the value is 3852.3 cm^{-1}. It has been used as reference to determine the nature of the shift in stretching OH_I frequency. For this analysis have been omitted N1, N2 and N3 because of the SA proton transfer and the cleavage of OH_I bond.

In Table 2 it can be observed that the values of $\Delta\nu_{OH\_I}$ are all negatives and span between -204 cm^{-1} (Cl0) and -1249 cm^{-1} (N0). It can be pointed out that a *redshift* of ν_{OH_I} is always associated to the hydrogen bond *HB* formation, as expected. In a same acceptor atom group, this effect enhances as the number of -CH$_3$ increases in the SA's partner molecule, except for F0 and F1 cases. In the F0 complex d_{NCI_I} is shorter than d_{HB} (1.79 and 1.84 Å respectively) . In addition, only in this case ρ_{NCI_I} is higher than ρ_{BCP_HB}: $\rho_{NCI\_I} = 0.0341$ e/bohr^3 > $\rho_{BCP\_HB} = 0.0283$ e/bohr^3. Then for what concern F0 complex it can be assumed that the NCI_I is a second hydrogen bond between the HF acid proton and the SA's oxygen (see Figure 1b) stronger than *HB*.

Regarding to the F1 complex, the substitution of the H for a methyl group leads to a NCI_I weaker between the methylic hydrogen atom and the SA's oxygen. The electron density values in NCI_I critical points (ρ_{NCI_I}) confirm this weakening: $\rho_{NCI\_I} = 0.0341$ for the F0 case, $\rho_{NCI\_I} = 0.0067$ e/a.u^3 for the F1 case.

P3 case is the case that shows the biggest $\Delta\nu_{OH\_I}$ (-967 cm^{-1}) although the P3 is characterized by

a d_{HB} length longer than the major part of the other complexes. The Frontier Molecular Orbital analysis shows the characteristic shapes of HOMOs orbitals for what concern the N and P acceptor atom groups (see Figure 4b). They are characterized by a big orbital lobe on the A atom which does not change its phase above and under the plane defined by the alkyl groups and A. Taking as interaction axis the one formed along the OH_I bond, the aspect above mentioned should permit a bigger overlap between the frontier orbitals $HOMO_{AX}$ and $LUMO_{SA}$.

As already mentioned in a previous paragraph, some difference has been encountered for what concern the trends of OH frequency shift in OH···O and OH···S associated to O2 and S2 cases. The observed and calculated OH stretching frequency redshift provided by Tang and Du[60-61] show, for the O–H···S bonded complexes that it was slightly larger than those for the O–H···O bonded complexes. The opposite results is obtained in our calculation. Although the ΔE_{HL} and the frontier molecular orbitals spatial distribution have been already proposed like starting points to unveil some aspects of the binding process (especially if SA's complexes characterized by acceptor atoms A belonging to the same chemical period are compared), it is reasonable to think that this redshift trend inconsistency could be due to the different molecular systems analyzed. If the H-donor is SA and the H-acceptor are DME or DMS, more than one non-covalent interaction are detectables. This fact induce us to think that the OH redshift should be considered as a overall effect of complexation. Once the complexation process succeeds, the E_b and the H-bond strength are not determined only by the ΔE_{HL}, but they are the result of a number of aspects that, in this study, have not been taken into deep consideration such as the molecular orbitals size, the overlap between the hydrogen acceptor atoms lone pairs and the SO-H antibonding orbital, the electronic density redistribution due to the complexation, etc.

As the OH_{II} bond is involved in the sequent steps of clusterization, the effect of the complexation on the acid OH_{II} bond has been analyzed. The OH_{II} bond strength affects the strength of further hydrogen bond that SA can provide like hydrogen donor molecule. The analysis of the d_{OH_II}

bond length, the ρ_{OH_II} and the $\Delta\nu_{OH\_II}$ shows that the formation of the major part gas phase binary clusters leads to a strengthening of OH_{II}, excepting for F0, Cl0 and Cl1. As can be seen in Table 2, there exist small d_{OH_II} variations. Nevertheless they can be considered indicators of different hydrogen acceptor molecules effects. As expected and shown in the same Table 2, d_{OH_II} decreases as ρ_{OH_II} increases. A linear relationship between the $\Delta\nu_{OH\_II}$ and ρ_{OH_II} is shown in Figure 6a). An increase of ρ_{OH_II} is generally associated to an increase of $\Delta\nu_{OH\_II}$. The plot can be divided in two zones: a *blueshift* zone ($\Delta\nu_{OH\_II} > 0$) and a *redshift* zone ($\Delta\nu_{OH\_II} < 0$). The major part of the complexes are characterized by a *blueshift* of ν_{OH_II} and it does mean that the OH_{II} in the complex is stronger than in the isolated SA molecule. On the contrary when the acceptor atom is a halogen (F, Cl) the complexation implies a weakening of OH_{II}, except in F1 case.

Figure 6b shows that there is a linear correlation between $\Delta\nu_{OH\_I}$ and $\Delta\nu_{OH\_II}$: as the redshift of the OH_I bond increases (*i.e.* $\Delta\nu_{OH\_I}$ takes more negative values and the bond weakens) the blueshift of OH_{II} bond also increases (*i.e.* $\Delta\nu_{OH\_II}$ more positive values and stronger bond). It could be argued that the *HB* formation permits an "electronic flow" from the *HB* region to OH_{II} through the SA molecule. This hypothesis is supported by the observation that this trend is particularly observed in a same group as the -CH_3 substitution increases, *i.e.* there are more electrons available to "flow" to OH_{II} bond.

The role of the NCI interactions cannot be forgotten for unraveling the reason of two kinds of OH_{II} stretching frequency shift. If the NCI_I interaction is not strong enough to recall the electronic "flow" on the hydrogen bond region the total effect is an increase of electron density in OH_{II} critical point and a consequent *blueshift* of ν_{OH_II}. Whereas when ρ_{NCI_I} takes values of a quite strong hydrogen bond (e.g. F0, Cl0) the flow of electron density remains on the SA side exposed to the bimolecular interaction and a total effect of weakening of OH_{II} occurs (i.e. *redshift* of ν_{OH_II}). Cl1 is characterized by two Non Covalent Interactions and it could explain why a *redshift* of ν_{OH_II} occurs also for this complex although ρ_{NCI} do not take values of a quite strong hydrogen bonds.

4. Conclusions and Future Perspectives

The nature of the gas phase binary clusterization between one molecule of H_2SO_4 and other eighteen molecules present in atmosphere has been studied. A systematic approach based on the nature of the hydrogen acceptor atom A and the degree of substitution (i.e. number of $-CH_3$ groups) of the SA partner molecule has been applied. The analysis has been carried out paying attention to the thermodynamic aspects of clusterization and to the factors that may affect the E_b binding energy of adducts formation. This energy is the result of a number of Non-Covalent Interactions between the two molecules. The contribution to the E_b amount which has been primarily analyzed is the one due to the H-bond formed between the SA's OH_I and the hydrogen acceptor atom A (i.e. N, O, F, P, S, Cl).

The Frontier Molecular Orbital analysis and the Atoms in Molecules characterization of the Electron Density function show that the Binding Energies are determined by two aspects mutually interconnected: the energy gap ΔE_{HL} between $LUMO_{SA}$ and $HOMO_{AX}$ and the electron density amount on the non-covalent interaction zones. Concerning to *HB* it has been observed that the electron density amount on the hydrogen bond critical point is function of the acceptor atom nature and can be modified by changing the number of $-CH_3$ groups directly bonded to A. The changes in ρ_{BCP_HB} are due to the energy gap ΔE_{HL} that shrinks as the $-CH_3$ number in the SA partner molecule gets bigger. This gap reduction would facilitate the formation of hydrogen bond crossing new MOs and a subsequent increasing of the electron density ρ_{BCP_HB}.

As a result of the *HB* formation, the weakening of the H-Donor bond (i.e acid OH_I bond) occurs. The rupture degree of SA's OH_I bond can be characterized by determining the loss of electron density ρ_{OH_I} and the *redshift* of the stretching frequency v_{OH_I}. Concerning the weakening of the OH_I bond, which has been taken as hydrogen bond *HB* strength descriptor, it can be concluded that the trimethylphosphine in P3 cluster ($\Delta v_{OH\_I}(P3) = 967,1$ cm^{-1}) is the chemical compound that approaches more the N0 case. It occurs although the H-bond electron density $\rho_{BCP\_HB}(P3) = 0.0417$ e/bohr^3 is

minor that the $\rho_{BCP\_HB}(O2) = 0.0599$ e/bohr^3 and the d_{HB_P3} length is 2,12 Å, bigger than $d_{HB\_O2} = 1.58$ Å. It highlights the importance of the orbitals symmetry concerning the overlap between the frontier molecular orbitals.

The gas phase binary cluster formation induces different changes in SA's OH_{II} bond depending on the SA partner molecule. They can affect the attachment of a third molecule to form a tri-molecular complex. The nature of these changes will be object of future studies.

Supporting Information Available

Cartesian coordinates of the optimized geometries, as xyz-files, and the calculated molecular orbitals description are available as supporting information. This material is available free of charge via the Internet at http://pubs.acs.org/

References

(1) Xiao, S.; Wang, M.Y.; Yao, L.; Kulmala, M.; Zhou, B.; Yang, X.; Chen, J.M.; Wang, D.F.; Fu, Q.Y.; Worsnop, D.R.; Wang, L. Strong Atmospheric New Particle Formation In Winter In Urban Shanghai, China. *Atmos. Chem. Phys.* **2015**, *15*, 1769–1781.

(2) Kulmala, M.; Vehkamäki H.; Petaja, T.; Dal Maso, M.; Lauri, A.; Kerminen, V.M.; Birmili, W.; McMurry, P.H. Formation And Growth Rates Of Ultrafine Atmospheric Particles: A Review Of Observations *J. of Aerosol Science* **2004**, *35*, 143–176.

(3) Kulmala, M.; Kerminen V.M. On The Formation And Growth Of Atmospheric Nanoparticles. *Atmospheric Research* **2008**, *90*, 132–150.

(4) Mirme, S; Mirme, A; Minikin, A; Petzold, A; Hõrrak, U.; Kerminen, V.M.; Kulmala, M. Atmospheric Sub-3 Nm Particles At High Altitudes. *Atmos. Chem. Phys.* **2010**, *10*, 437–451.

(5) Zhang, R; Khalizov, A; Wang, L.; Hu, M.; Xu, W. Nucleation And Growth Of Nanoparticles In The Atmosphere. *Chem.Rev.* **2012**, *112*, 1957-2011.

(6) O'Dowd, C.D.; Jimenez, J.L.; Bahreini, R.; Flagan, R.C.; Seinfeld, J.H.; Hämeri, K; Liisa Pirjola, L.; Kulmala, M.; Jennings, S.G.; Hoffmann, T. Marine Aerosol Formation From Biogenic Iodine Emissions. *Nature* **2002,** *417*, 632-636.

(7) Park, J.; Sakurai, H.; Vollmers, K.; McMurry, P.H. Aerosol Size Distributions Measured At The South Pole During ISCAT. *Atmos.Environ.*, **2004**, *38*, 5493–5500.

(8) Dal Maso, M.; Kulmala, M.; Riipinen, I.; Wagner, R.; Hussein, T.; Aalto, P.P.; Lehtinen, K.E.J. Formation And Growth Of Fresh Atmospheric Aerosols: Eight Years Of Aerosol Size Distribution Data From SMEAR II, Hyytiälä, Finland *Boreal. Environ. Res.* **2005,** *10*, 323–336.

(9) Kanawade, V.P.; Benson, D.R.; Lee, S.-H. Statistical Analysis Of 4-year Observations Of Aerosol Sizes In A Semirural Continental Environment. *Atmos. Environ.* **2012**, *59*, 30–38.

(10) Dunn, M.J.; Jiménez, J.L.; Baumgardner, D.; Castro, T.; McMurry, P.H.; Smith, J.N. Measurements Of Mexico City Nanoparticle Size Distributions: Observations Of New Particle Formation And Growth *Geophys. Res. Lett.* **2004**, *31*, L10102.

(11) Dunne E.M. et al.; Global Atmospheric Particle Formation From CERN CLOUD Measurements. *Science* **2016**, *354 (6316)*, 119-1124.

(12) Eisele, F.L.; Tanner, D.J. Measurement Of Gas Phase Concentration Of H_2SO_4 And Methanesulfonic Acid And Estimates Of H_2SO_4 Production And Loss In The Atmosphere. *J. Geophys. Res.* **1993,** *98*, 9001–9010.

(13) Stolzenburg, M.R.; McMurry, P.H. An Ultrafine Aerosol Condensation Nucleus Counter. *Aerosol Sci. Technol.* **1991**, *14*, 48–65.

(14) Kirkby J. et al.; Role Of Sulphuric Acid, Ammonia And Galactic Cosmic Rays In Atmospheric Aerosol Nucleation. *Nature* **2011**, *476*, 429–433.

(15) Bandy, A.R.; Ianni, J.C. Study Of The Hydrates Of H_2SO_4 Using Density Functional Theory. *J. Phys. Chem. A* **1998**, *102*, 6533-6539.

(16) Ianni, J.C.; Bandy A.R. A Theoretical Study Of The Hydrates Of $(H_2SO_4)_2$ And Its

24

Implications For The Formation Of New Atmospheric Particles. *J. Mol. Structure (Theochem)* **2000**, *497*, 19–37.

(17)   Kurtén, T.; Loukonen, V.; Vehkamäki, H.; Kulmala, M. Amines Are Likely To Enhance Neutral And Ion-induced Sulfuric Acid-water Nucleation In The Atmosphere More Effectively Than Ammonia. *Atmos. Chem. Phys.* **2008**, *8*, 4095–4103.

(18)   Berndt, T. et al. Laboratory Study On New Particle Formation From The Reaction OH + SO_2 : Influence Of Experimental Conditions, H_2O Vapour, NH_3 And The Amine Tert-butylamine On The Overall Process. *Atmos. Chem. Phys.* **2010**, *10*, 7101–7116.

(19)   Loukonen, V.; Kurtén, T.; Ortega, I.K.; Vehkamäki, H.; Pádua, A.A.H.; Sellegri, K.; Kulmala, M. Enhancing Effect Of Dimethylamine In Sulfuric Acid Nuclation In The Presence Of Water – A Computational Study. *Atmos. Chem. Phys.* **2010**, *10*, 4961–4974.

(20)   Berndt, T.; Sipilä, M.; Stratmann, F.; Petäjä T.; Vanhanen, J.; Mikkilä, J.; Patokoski, J.; Taipale, R.; Mauldin III, R.L.; Kulmala, M. Enhancement Of Atmospheric H_2SO_4/H_2O Nucleation: Organic Oxidation Products Versus Amines. *Atmos. Chem. Phys.* **2014**, *14*, 751–764.

(21)   Facchini, M.C. et al. Important Source of Marine Secondary Organic Aerosol From Biogenic Amines. *Environ. Sci. Technol.* **2008**, *42*, 9116−9121.

(22)   Sorooshian, A. et al. On The Link Between Ocean Biota Emissions, Aerosol, and Maritime Clouds: Airborne, Ground, and Satellite Measurements Off the Coast of California. *Glob. Biogeochem. Cycles* **2009**, *23*, GB4007.

(23)   Chen, H.; Ezell, M.J.; Arquero, K.D.; Varner, M.E.; Dawson, M.L.; Gerber, R.B.; Finlayson-Pitts, B.J. New Particle Formation and Growth from Methanesulfonic Acid, Trimethylamine and Water. *Phys. Chem. Chem. Phys.* **2015**, *17*, 13699−13709.

(24)   Chen, H.; Varner, M.E.; Gerber, R.B.; Finlayson-Pitts, B.J. Reactions Of

Methanesulfonic Acid With Amines And Ammonia As A Source Of New Particles In The Air. *J. Phys. Chem. B* **2016**, *120 (8)*, 1526-1536.

(25)   Chen, H.; Finlayson-Pitts, B.J. New Particle Formation from Methanesulfonic Acid and Amines/Ammonia as a Function of Temperature *Environ. Sci. Technol.*, **2017**, *51 (1)*, 243–252.

(26)   Dawson, M.L.; Varner, M.E.; Perraud, V.; Ezell, M.J.; Gerber, R.B.; Finlayson-Pitts, B.J. Simplified Mechanism for New Particle Formation from Methanesulfonic Acid, Amines, and Water via Experiments and Ab Initio Calculations. *Proc.Natl.Acad.Sci.* **2012**,*109*, 18719-18724

(27)   Dawson, M.L.; Varner, M.E.; Perraud, V.; Ezell, M.J.; Wilson, J.; Zelenyuk, A.; Gerber, R.B.; Finlayson-Pitts, B.J. Amine-Amine Exchange in Aminium-Methanesulfonate Aerosols. J. Phys. Chem. C **2014**, *118*, 29431-29440.

(28)   Barnes, I.; Hjorth, J.; Mihalopoulos, N. Dimethyl Sulfide and Dimethyl Sulfoxide and Their Oxidation in the Atmosphere. *Chem. Rev.* **2006**, *106*, 940-975.

(29)   Perraud, V. et al. The Future of Airborne Particles in the Absence of Fossil Fuel Sulfur Dioxide Emissions. *Proc. Natl. Acad. Sci. U. S. A.* **2015**, *112*, 13514-13519.

(30)   Bork, N.; Elm, J.; Olenius, T.; Vehkamäki, H.; Methane sulfonic acid-enhanced formation of molecular clusters of sulfuric acid and dimethyl amine. *Atmos. Chem. Phys.* **2014**, *14*, 12023–12030.

(31)   Kumar, M.; Francisco, J.S. Ion Pair Particles At The Air–water Interface *Proc. Natl. Acad. Sci.* **2017,** *114*, 12401-12406.

(32)   Kumar, M.; Sinha, A.; Francisco, J.S. Role of Double Hydrogen Atom Transfer Reactions in Atmospheric Chemistry *Acc. Chem. Res.* **2016**, *49*, 877–883.

(33)   Anglada, J.M.; Olivella, S.; Solé, A. Hydrogen Transfer Between Sulfuric Acid and

Hydroxyl Radical in the Gas Phase: Competition Among Hydrogen Atom Transfer, Proton-Coupled Electron-Transfer, and Double Proton Transfer. **2006**, *110*, 1982-1990.

(34)   Schmidt, M.W.; Baldridge, K.K.; Boatz, J.A.; Elbert, S.T.; Gordon, M.S.; Jensen, J.H.; Koseki, S.; Matsunaga, N.; Nguyen, K.A.; Su, S.; Windus, T.L.; Dupuis, M.; Montgomery, J.A. General Atomic and Molecular Electronic Structure System. *J. Comput. Chem.* **1993**, *14*, 1347-1363.

(35)   *Theory and Applications of Computational Chemistry: the first forty years*; Gordon, M.S., Schmidt, M.W.; Dykstra, C.E.; Frenking, G.; Kim, K.S.; Scuseria, G.E. (editors), Elsevier: Amsterdam, 2005.

(36)   Chai, J.; Head-Gordon, M. Long-range Corrected Hybrid Density Functionals With Damped Atom–atom Dispersion Corrections. *Phys. Chem. Chem. Phys.* **2008**, *10*, 6615–6620.

(37)   Elm, J.; Bilde, M.; Mikkelsen, K.V. Assessment Of Binding Energies Of Atmospherically Relevant Clusters. *Phys. Chem. Chem. Phys.* **2013**, *15*, 16442-16445.

(38)   Elm, J.; Kristensen, K. Basis Set Convergence Of The Binding Energies Of Strongly Hydrogen-bonded Atmospheric Clusters. *Phys. Chem. Chem. Phys.* **2017**, *19*, 1122-1133.

(39)   Elm, J.; Mikkelsen, K.V. Computational Approaches For Efficiently Modelling Of Small Atmospheric Clusters. *Chem. Phys. Let.* **2014**, *615*, 26-29.

(40)   Bode, B. M.; Gordon, M. S. Macmolplt: A Graphical User Interface For GAMESS *J. Mol. Graphics and Modeling*, **1999**, *16*, 133-138.

(41)   Lu, T.; Chen, F.J. Multiwfn: A Multifunctional Wavefunction Analyzer. *Comp. Chem.* **2012,** 33, 580-592.

(42)   Elm, J.; Jen, C.N; Kurtén, T.; Vehkamäki, H. Strong Hydrogen Bonded Molecular Interactions Between Atmospheric Diamines And Sulfuric Acid. *J. Phys. Chem. A.* **2016**, *120*, 3693–3700.

(43)   Olenius, T.; Halonen, R.; Kurtén, T.; Henschel, H.; Kupiainen-Määtta, O.; Ortega, I.K.;

Jen, C.N.; Vehkamäki, H.; Riipinen, I. New Particle Formation From Sulfuric Acid and Amines: Comparison of Mono-, Di-, and Trimethylamines. *J. Geophys. Res. Atmos* **2017**, *122*, 7103–7118.

(44)   Jen, C.N.; Bachman, R.; Zhao, J.; McMurry, P.H. Diamine-sulfuric Acid Reactions Are A Potent Source Of New Particle Formation. *Geophys. Res. Lett.* **2016**, *43*, 867-873.

(45)   *Atoms In Molecules: A Quantum Theory.*   Bader R. F.W; Clarendon Press: Oxford, 1999.

(46)   Dimitrova, V.; Ilieva, S.; Galabov, B. Electrostatic Potential At Nuclei As A Reactivity Index In Hydrogen Bond Formation. Complexes Of Ammonia With C–H, N–H And O–H Proton Donor Molecules. *J. Mol. Structure (Theochem)* **2003**, *637*, 73–80.

(47)   Galabov, B.; Bobadova-Parvanova, P.; Ilieva, S.; Dimitrova, V. The Electrostatic Potential At Atomic Sites As A Reactivity Index In The Hydrogen Bond Formation. *J. Mol. Structure (Theochem).* **2003,** *630*, 101–112.

(48)   *Chemical Applications of Atomic and Molecular Electrostatic Potentials.* Politzer, P., Trulhar D.G.; SPRINGER SCIENCE BUSINESS MEDIA, LLC.: New York, **1981.**

(49)   *The Nature Of The Hydrogen Bond Outline Of A Comprehensive Hydrogen Bond Theory* Gilli, G., Gilli, P.;   *Oxford University Press*: New York, **2009.**

(50)   Gilli, G.; Gilli, P. Towards An Unified Hydrogen-bond Theory. *J. Mol. Structure* **2000**, *552*, 1-15.

(51)   Eisele, F.L.; Hanson, D.R. First Measurement Of Prenucleation Molecular Clusters Atmospheric Chemistry Division. *J. Phys. Chem. A*. **2000**, *104* (4), 830–836.

(52)   Elm, J.; Bilde, M.; Mikkelsen, K.V. Influence Of Nucleation Precursors On The Reaction Kinetics Of Methanol With The OH Radical   *J. Phys. Chem. A* **2013**, *117*, 6695–6701.

(53)   Elm, J.; Myllys, N.; Kurtén, T. What Is Required for Highly Oxidized Molecules To Form Clusters with Sulfuric Acid? *J. Phys. Chem. A* **2017**, *121*, 4578–4587.

(54)   Wang, B.; Jiang, W.; Dai, X.; Gao, Y.; Wang, Z.; Zhang, R.-Q. Molecular Orbital Analysis Of The Hydrogen Bonded Water Dimer. *Nature Scientific Reports 6*   **2016** Article number: 22099.

(55)   Parthasarathi, R.; Sundar Raman, S.; Subramanian, V.; Ramasami, T. Bader's Electron Density Analysis Of Hydrogen Bonding In Secondary Structural Elements Of Protein. *J. Phys. Chem. A* **2007**, *111*, 7141-7148.

(56)   Grabowski, S.J. What Is The Covalency Of Hydrogen Bonding? *Chem. Rev.* **2011**, *111*, 2597–2625.

(57)   Rozenberg, M. The Hydrogen Bond - Practice And QTAIM Theory *Royal Society of Chemistry Adv.* **2014,** *4*, 26928-26931.

(58)   Zou, J.-W.; Huang, M.; Hu G.-X.; Jiang, Y.J.   Toward A Uniform Description Of Hydrogen Bonds And Halogen Bonds: Correlations Of Interaction Energies With Various Geometric, Electronic And Topological Parameters. *Royal Society of Chemistry Adv.* **2017**, *7*, 10295-10305.

(59)   Popelier, P.L.A. Characterization Of A Dihydrogen Bond On The Basis Of The Electron Density. *J. Phys. Chem. A* **1998**, *102*, 1873-1878.

(60)   Tang, S.; Zhao, H.; Du, L. Hydrogen Bonding In Alcohol–ethylene Oxide And Alcohol–ethylene Sulfide Complexes. *Royal Society of Chemistry Adv*. **2016,** *6*, 91233-91242

(61)   Du, L.; Tang, S.; Hansen, A.S.; Frandsen, B.N.; Maroun, Z.; Kjaergaard, H.G. Subtle Differences In The Hydrogen Bonding Of Alcohol To Divalent Oxygen And Sulfur. *Chem. Phys. Lett* **2017**, *667*, 146-153

1
2
3
4
5
6
7
8
9
10
11
12
13
14
15
16
17
18
19
20
21
22
23
24
25
26
27
28
29
30
31
32
33
34
35
36
37
38
39
40
41
42
43
44
45
46
47
48
49
50
51
52
53
54
55
56
57
58
59
60

Table 1. Binary Molecular Complexes

	Nitrogen	Oxygen	Fluorine	Phosphorus	Sulfur	Clhorine
Id: No-Substitution	N0: H_2SO_4-(NH_3)	O0: H_2SO_4-H_2O	F0: H_2SO_4-HF	P0: H_2SO_4-PH_3	S0: H_2SO_4-H_2S	Cl0: H_2SO_4-HCl
Id: Mono-Substituted	N1: H_2SO_4-$(CH_3)NH_2$	O1: H_2SO_4-$(CH_3)OH$	F1: H_2SO_4-CH_3F	P1: H_2SO_4-$(CH_3)PH_2$	S1: H_2SO_4-$(CH_3)SH$	Cl1: H_2SO_4-$(CH_3)Cl$
Id: Bi-Substituted	N2: H_2SO_4-$(CH_3)_2NH$	O2: H_2SO_4-$(CH_3)_2O$		P2: H_2SO_4-$(CH_3)_2PH$	S2: H_2SO_4-$(CH_3)_2S$	
Id: Tri-Substituted	N3: H_2SO_4-$(CH_3)_3N$			P3: H_2SO_4-$(CH_3)_3P$		

Binary complexes divided according to the acceptor atom A group and partner molecule's degree of

substitution (i.e. number of -CH_3 groups).

1
2
3
4
5
6
7
8
9
10
11
12
13
14
15
16
17
18
19
20
21
22
23
24
25
26
27
28
29
30
31

Table 2. Complete List of Simulation Results

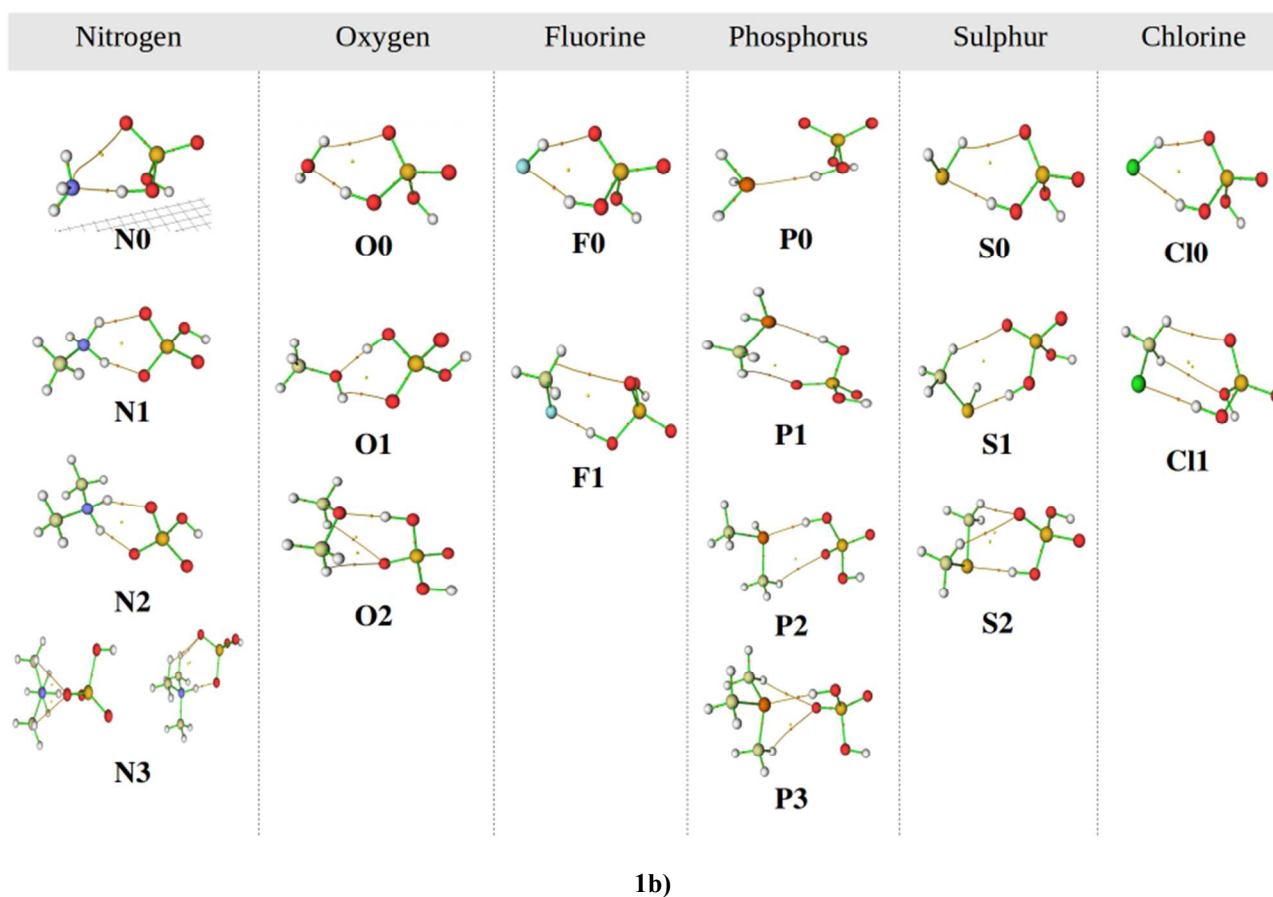| Id.	d_{HB}	d_{OH_I}	Δd_{OH_I}	d_{OH_II}	Δd_{OH_II}	d_{NCI_I}	E_b DFT / CC	ΔG	ΔH	$T\Delta S$	ΔE_{HL}	ρ_{BCP_HB}	$\nabla^2 \rho_{BCP\_HB}$	ρ_{NCI_I}	ρ_{NCI_II}	ρ_{RCP_I}	ρ_{RCP_II}	ρ_{OH_I}	ρ_{OH_II}	Δv_{OH_I}	Δv_{OH_II}	V_H
SA	-	0.964	-	0.964	-	-	-	-	-	-	-	-	-	-	-	-	-	0.3665	0.3665	-	-	-
N0	1.610	1.030	0.064431	0.962	-0.001569	3.070	16.72 / 16.57	-7.33	-17.07	-9.74	0.3830	0.0683	0.0744	0.0097	-	0.0097	-	0.2921	0.3683	-1249.08	8.29	-0.9538
N1	1.060	1.610	0.643431	0.961	-0.002569	1.774	20.16 / 20.77	-9.43	-19.36	-9.93	0.3514	0.3209	-0.1830	0.2994	0.0588	0.0169	-	0.0402	0.3705	-	16.05	-0.9584
N2	1.050	1.680	0.719431	0.961	-0.002569	1.715	23.09 / 25.13	-11.46	-22.58	-11.12	0.3336	0.3154	-1.8090	0.3195	0.0494	0.0167	-	0.0459	0.3707	-	30.91	-0.9693
N3	1.080	1.500	0.533431	0.961	-0.002769	2.411	25.18 / 27.62	-13.87	-24.33	-10.46	0.3239	0.2872	-1.5500	0.0118	0.0118	0.0087	0.0087	0.0775	0.3711	-	32.97	-0.9766
O0	1.680	0.990	0.029431	0.963	-0.000569	2.215	12.63 / 12.94	-3.31	-12.77	-9.45	0.4350	0.0462	0.1241	0.0151	-	0.0119	-	0.3282	0.3671	-590.35	2.31	-0.9347
O1	1.630	1.000	0.038431	0.963	-0.000569	2.268	13.89 / 14.6	-4.43	-14.13	-9.71	0.3929	0.0553	0.1300	0.0151	-	0.0124	-	0.3183	0.3672	-768.15	5.42	-0.9385
O2	1.580	1.010	0.041431	0.963	-0.000669	2.720	14.4 / 15.59	-4.05	-14.60	-10.55	0.3723	0.0599	0.1351	0.0062	0.0063	0.0056	0.0058	0.3151	0.3678	-863.84	5.70	-0.944
F0	1.840	0.980	0.013455	0.964	0.000414	1.791	10.32 / 10.90	-1.88	-10.80	-8.92	0.5379	0.0283	0.0982	0.0341	-	0.014	-	0.3477	0.3655	-264.58	-7.59	-0.9104
F1	1.740	0.980	0.013485	0.963	-0.000262	2.768	8.36 / 9.27	-0.41	-8.76	-8.36	0.4649	0.0326	0.1160	0.0067	-	0.005	-	0.3476	0.3670	-263.59	0.45	-0.9315
P0	2.310	0.980	0.020741	0.963	-0.000368	-	6.57 / 7.11	0.89	-7.06	-7.96	0.3859	0.0253	0.0383	-	-	-	-	0.3415	0.3296	-415.12	1.94	-0.9197
P1	2.240	0.990	0.029156	0.963	-0.000453	2.724	9.62 / 10.07	-0.29	-10.18	-9.89	0.3599	0.0312	0.0373	0.0059	-	0.0054	-	0.3309	0.3675	-602.71	3.15	-0.9415
P2	2.180	1.000	0.037427	0.963	-0.000599	2.715	11.17 / 11.46	-4.11	-13.64	-9.53	0.3419	0.0361	0.0340	0,0060	-	0.0053	-	0.3218	0.3678	-773.00	5.84	-0.9489
P3	2.120	1.010	0.048243	0.963	-0.000723	2.813	13.45 / 14.22	-3.58	-14.16	-10.59	0.3289	0.0417	0.0281	0.0049	0.0053	0.0052	-	0.3107	0,3680	-967.16	7.42	-0.9533
S0	2.250	0.980	0.019611	0.963	-0.000226	2.606	7.45 / 8.05	2.15	-6.21	-8.36	0.3743	0.0263	0.0469	0.0081	-	0.0069	-	0.3416	0.3670	-409.11	0.10	-0.9317
S1	2.170	0.990	0.027761	0.963	-0.000292	2.492	10.19 / 10.80	-1.03	-10.74	-9.71	0.3475	0.0324	0.0473	0.0087	-	0.0059	-	0.3322	0.3672	-572.07	1.10	-0.9371
S2	2.100	1.000	0.036731	0.963	-0.000439	2.550	12.59 / 13.27	-3.26	-13.28	-10.02	0.3269	0.0390	0.0445	0.0078	0.0078	0.0052	0.0051	0.3222	0.3674	-754.00	2.00	-0.9422
Cl0	2.330	0.980	0.013168	0.964	0.000271	2.050	6.27 / 7.29	1.06	-7.12	-8.19	0.4469	0.0184	0.0503	0.0205	-	0,0090	-	0.3527	0.3659	-204.00	-6.13	-0.914
Cl1	2.210	0.980	0.014431	0.964	-0.000054	2.972	7.29 / 7.16	0.66	-7.84	-8.50	0.4099	0.0244	0.0577	0.0082	0.0033	-	-	0.3476	0.3669	-294.00	-2.89	-0.9281
	Geometrical Parameters						**Thermodynamic quantities**				**M.O. Energy gap**	**AIM Analysis**								**Frequency shift**		**E. Potential**

Simulation Data - Id: Identification code of molecular system; **Geometrical Parameters** (in Å) :

hydrogen bond length d$_{HB}$, OH bond lengths d$_{OH\_II}$ and d$_{OH\_II}$, NCI$_I$ bond length d$_{NCI\_I}$ and the

corresponding variation Δd; **Thermodynamic Functions** (kcal/mol): Binding Energy E$_b$ (from DFT

and Coupled Cluster (CC) calculations), Gibbs Free Energy of formation ΔG, Enthalpy of formation

ΔH, TΔS contribution; **Frontier Molecular Orbital Energy gap** (a.u.) ΔE_{HL}; **AIM Parameters**:

electron density at hydrogen bond critical point ρ_{BCP_HB} and Laplacian $\nabla^2\rho_{BCP\_HB}$, at OH critical

points ρ_{OH_I} and ρ_{OH_II}, at no covalent interaction critical point ρ_{NCI_I} and ρ_{NCI_II}, at ring critical points

ρ_{RCP_I} and ρ_{RCP_II} (e/bohr^3): electron density in Bond Critical Points and Ring Critical Points;

Stretching Frequency Shift (cm^{-1}): corresponding to OH bonds, Δv_{OH_I} and Δv_{OH_II}; **Electrostatic**

Potential: at SA's hydrogen nucleus (a.u.): V_H

1a)

Nitrogen	Oxygen	Fluorine	Phosphorus	Sulphur	Chlorine

1b)
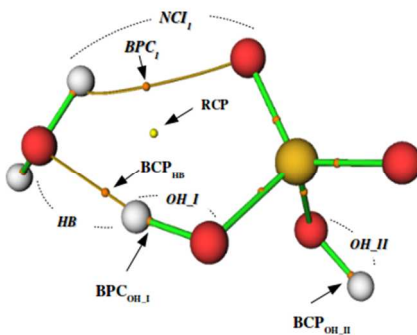
Figure 1. a) Example of gas phase binary complex - Case of $H_2O + H_2SO_4$: *HB* is the main hydrogen

bond; *NCI_I* is a further Non-Covalent interaction; OH_I is the O-H bond which participates in the

hydrogen bond SOH...Acceptor Atom; OH_{II} is the O-H bond free of interactions on the opposite side of

the SA. BCP and RCP are Bond Critical and Ring Critical Points respectively.

b) Optimized structures and Molecular graphs.

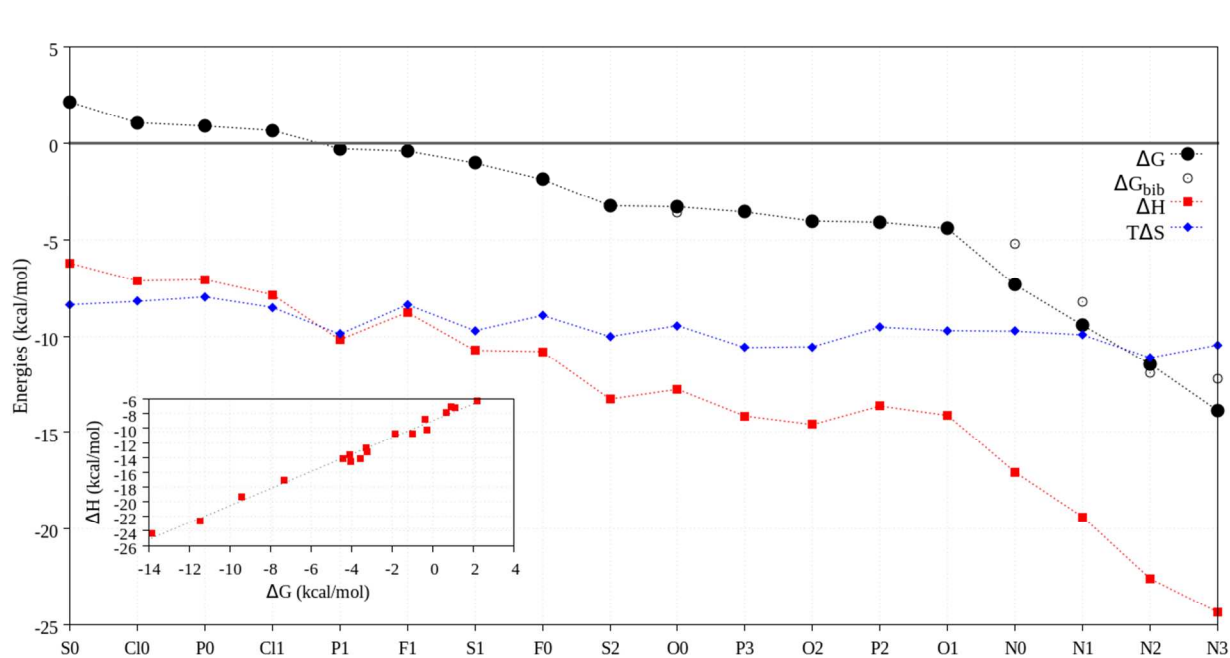**Figure 2**. Values of ΔG ordered in decreasing mode: entropy and enthalpy contributions are depicted

for each case. Circles (•,○): ΔG values: from simulation and bibliography (Reference 42,51)
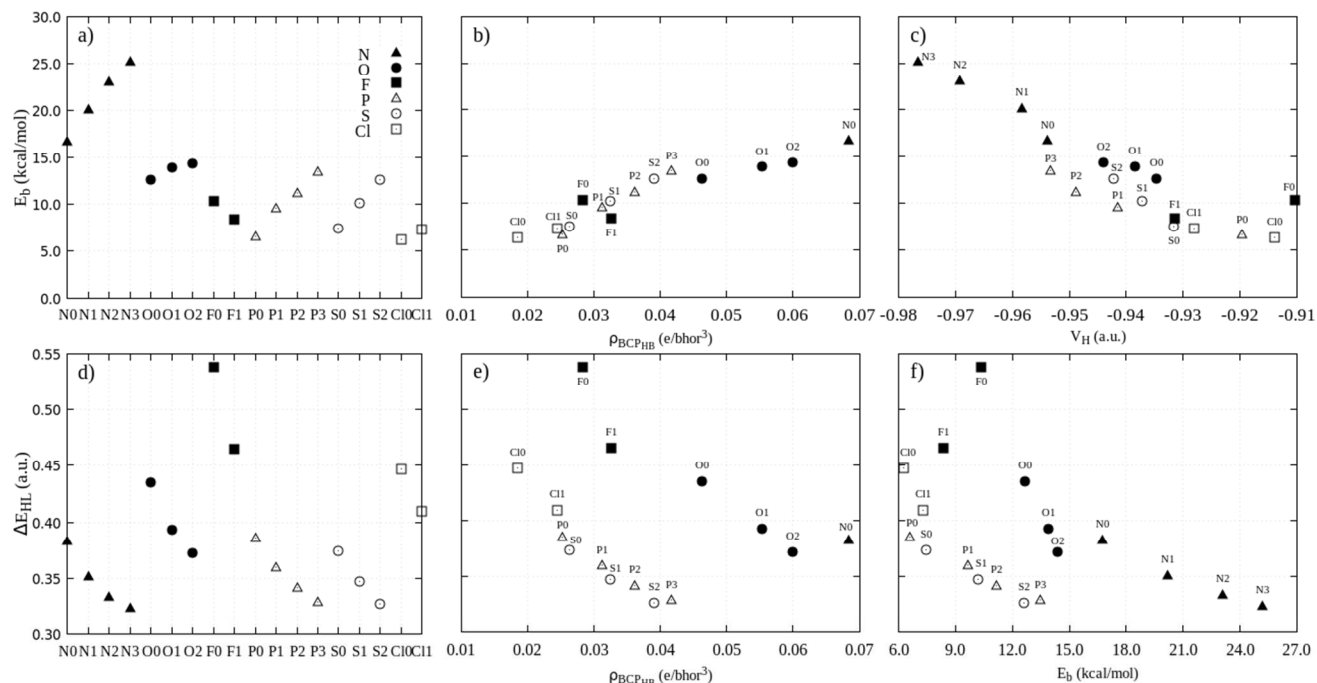
respectively; (·): ΔH values; (♦): TΔS values.

Figure 3. a) Binary cluster binding energies E_b (kcal/mol); **b)** Relation between ρ_{BCP_HB} (e/bohr^3) and E_b; **c)** Relation between V_H (a.u.) and E_b; **d)** Frontier molecular HOMO$_{AX}$-LUMO$_{SA}$ gap energy ΔE_{HL} (a.u.); **e)** Relation between ρ_{BCP_HB} and ΔE_{HL}; **f)** Relation between E_b and ΔE_{HL}

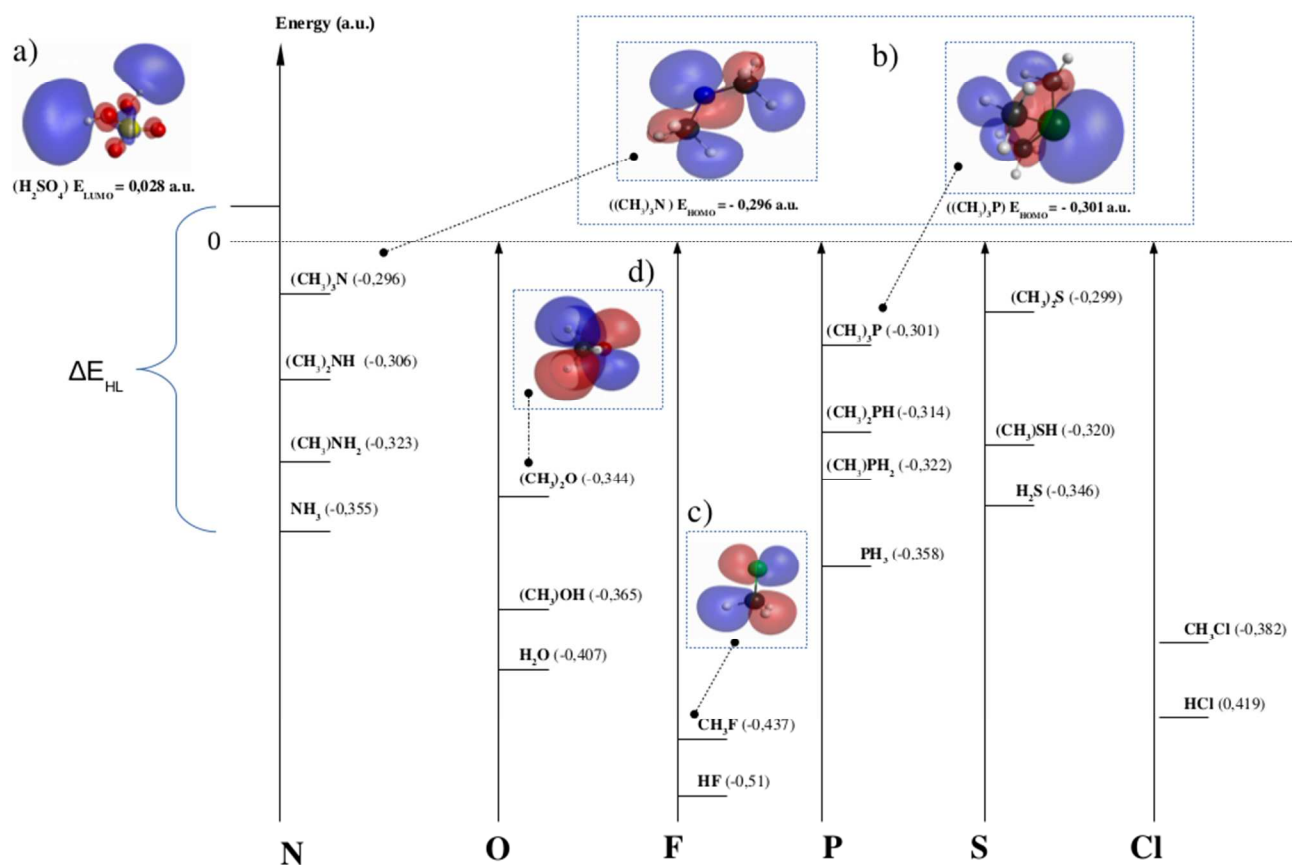**Figure 4.** Molecular Orbitals: **a)** Sulfuric acid LUMO description; **b)** Examples of partner molecule

HOMOs description; **c)** $(CH_3)F$ HOMO description; **d)** $(CH_3)_2O$ HOMO description. The diagram

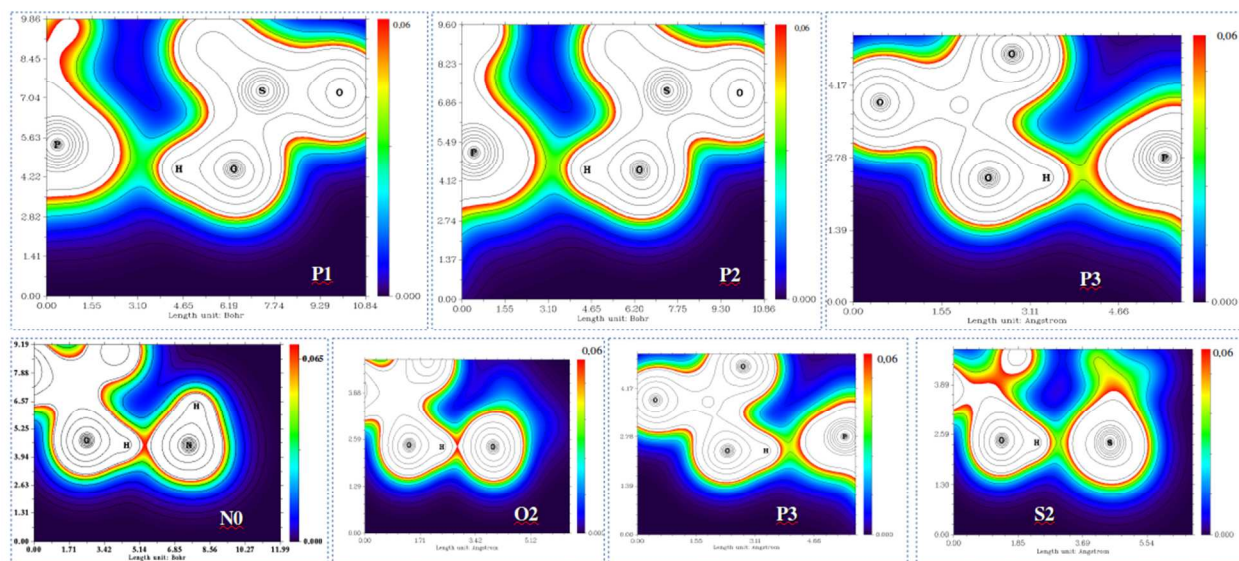shows the partner molecule HOMOs energies (a.u.)

Figure 5. Electron density map on the hydrogen bond plane for different bimolecular clusters. In each case the lower and upper electron density values are 0.0 (dark blue) and 0.6 a.u. (intense red) respectively, except for the N0 case (0.0 and 0.065 a.u.).
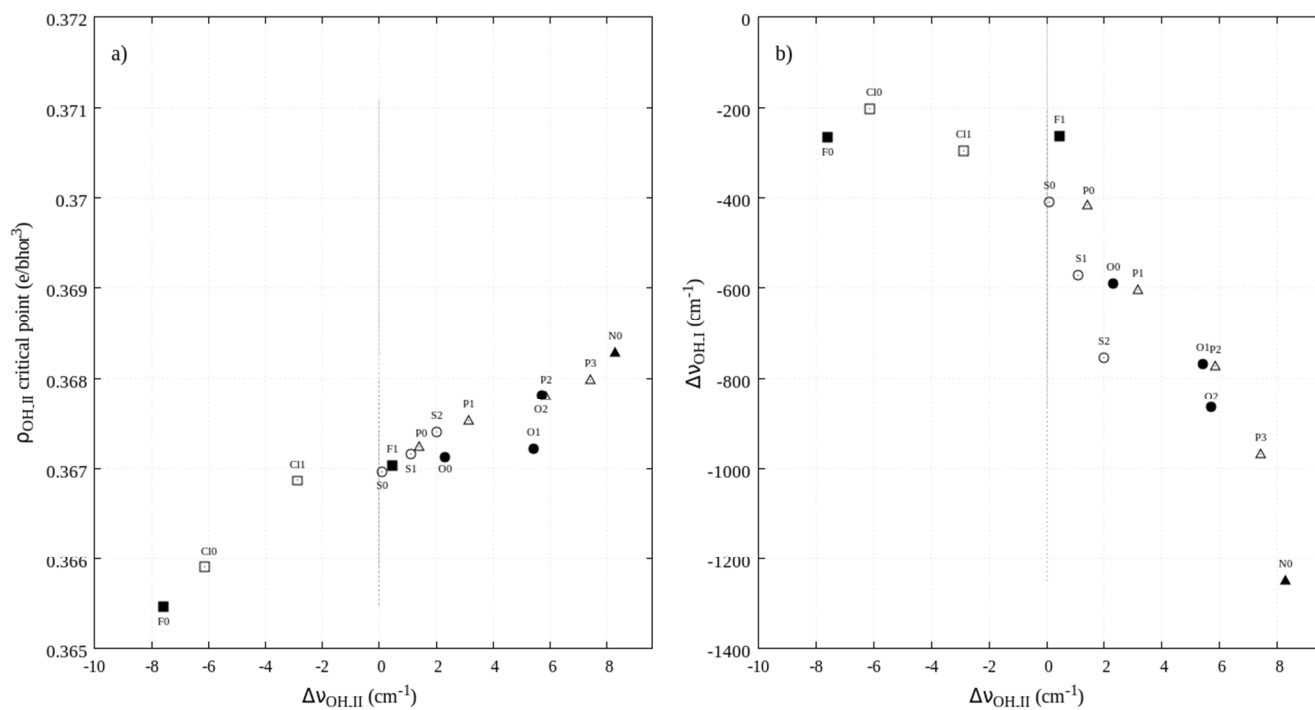
Figure 6. a) OH_{II} stretching frequency shift as function of electron density in OH_{II} critical point.

b) $\Delta\nu_{OH\_II}$ stretching frequency shift vs $\Delta\nu_{OH\_I}$ stretching frequency shift.

TOC Graphic

$\Delta \nu_{OH\_I} = -967$ cm^{-1}

$E_b = 13,45$ kcal/mol

$\Delta G = -3,58$ kcal/mol

HOMO((CH$_3$)$_3$P) = -0.301 a.u.

LUMO(H$_2$SO$_4$) = 0.028 a.u.

$\Delta \nu_{OH\_I} = -863$ cm^{-1}

$E_b = 14,45$ kcal/mol

$\Delta G = -4,05$ kcal/mol

HOMO ((CH$_3$)$_2$O) = -0.344 a.u.

LUMO(H$_2$SO$_4$) = 0.028 a.u.